RSC Advances

PAPER

View Article Online
View Journal | View Issue

Cite this: *RSC Adv.*, 2019, **9**, 41438

Polyurethane-based bionic material simulating the Vis-NIR spectrum and thermal infrared properties of vegetation

Anran Hu, Min Li,* Liping Zhang, Chunxia Wang and Shaohai Fu*

Poor stability, the toxicity of the used colorants and complex structure are the main problems for the current spectral simulation materials for vegetation. In this paper, a lightweight (0.052 g cm^{-3}) and environmentally friendly bionic porous spectrum simulation material (BPSSM) was developed to simulate the Vis-NIR spectra of natural leaves. The porous structure of BPSSM was used to simulate the mesophyll tissue, which endows the BPSSM with a near-infrared plateau. Moreover, the relationship between pore structure (size, open porosity and volume density) and near-infrared plateau in the spectrum was also studied. The chlorophyll of leaves was simulated by vat dyes or organic pigments, and the green apex and red edge characteristics in the visible region were further adjusted by the chlorophyllin sodium copper salt. The water absorption of BPSSM with 100–120% water contents are consistent with the natural leaves spectral curve channel. Finally, the spectral correlation coefficients (r_m) between BPSSM and different natural leaves are up to 0.984, suggesting that the BPSSM is universally applicable for the simulation of different leaves. Interestingly, the average radiant temperature difference between BPSSM and natural leaves is 0.25 °C within 24 hours, indicating it has similar thermal infrared properties to natural leaves. Moreover, the BPSSM can be combined with textiles to obtain a composite fabric, and its breaking strength and photostability were explored.

Received 12th October 2019
Accepted 9th December 2019

DOI: 10.1039/c9ra08312j

rsc.li/rsc-advances

1. Introduction

Hyperspectral imaging technology can identify targets in an environment background through spectral nuances ranging from 380–2500 nm.[1] Different ground objects exhibit distinct spectral characteristics due to the divergences in composition and structure. Since vegetation is the most common environment background, it is significant to develop materials that can simulate the spectral characteristics of natural leaves to counter hyperspectral detection.[2–4] In this regard, some researchers have developed dyed fabrics by using dyes with similar spectral properties to green leaves. However, the spectra of these roughly match with leaves merely in the range of 380–1300 nm with poor spectral similarity.[5–8]

To further simulate the spectra of natural leaves within 380–2500 nm, researchers have attempted to prepare a bionic leaf that mimics the Vis-NIR spectra of the leaves by simulating their structure and composition. Liu *et al.* proposed a bionic leaf model that uses polymer film, polyurethane foam material, chlorophyll microcapsule and super absorbent resin to simulate the epidermal layer, loose porous mesophyll tissue, chloroplast and water of leaves, respectively.[9] Yang *et al.* encapsulated chlorophyll into polyvinyl alcohol film, and composited with transparent polyvinyl chloride, a sealed bag of polyvinylidene chloride (PVDC) containing water and paper to prepare bionic leaf.[10] However, the preparation processes as well as the multilayer structures of these bionic leaves are complicated, which limits its application.

Considering these issues, Qin *et al.* prepared green poly(-urea–formaldehyde) microcapsules with similar reflectance spectrum in Vis-NIR region to leaves, which was expected to be applied to spectral simulation materials.[11] Chlorophyll was widely used in these materials to simulate spectral characteristics of natural leaves in the visible region, but its stability is poor and it is easy to decompose.[12,13] Chrome oxide green has outstanding stability and similar reflectance characteristics to chlorophyll, which is commonly used for spectral simulation materials to replace chlorophyll.[14,15] Gao *et al.* developed a bionic leaf with polyvinyl alcohol as the main component, lithium chloride and chrome oxide green as additives. The spectral correlation coefficients between the bionic leaf and two kinds of leaves are over than 0.95.[16] Since chrome oxide green is toxic and increases the weight of the materials,[17,18] it is significative to explore environmentally friendly colorants that mimic the spectra of leaves.

In this paper, a lightweight and environmentally friendly polyurethane-based bionic porous spectrum simulation material (BPSSM) was designed inspired by the structure and

Jiangsu Engineering Research Center for Digital Textile Inkjet Printing, Key Laboratory of Eco-Textile, Jiangnan University, Ministry of Education, Wuxi, Jiangsu 214122, China. E-mail: minmin0421@163.com; shaohaifu@hotmail.com

composition of natural leaves. Four reflection spectral features (near-infrared plateau, green apex, red edge and water absorption valley) of natural leaves in Vis-NIR region were simulated. The polyurethane-based bionic porous substrate (BPS) was used to simulate the near-infrared plateau characteristics of mesophyll tissue. Environmentally friendly colorants and water were used to imitate the function of chlorophyll and water in leaves, which endowed the BPSSM green apex, red edge and water absorption valley in spectrum. Significantly, the BPSSM exhibits similar Vis-NIR spectrum and thermal infrared property with natural leaves, which is expected to be combined with textiles for apparel against hyperspectral detection, and its application performance was preliminary explored.

2. Experimental

2.1 Materials

Polyether polyol 3050 (hydroxyl value is 54.5–57.5 mg_{KOH} g^{-1}, ≥99.0%), toluene diisocyanate (TDI 80/20, $C_{18}H_{12}N_4O_4$, ≥99.0%) and stannous octoate T9 (catalyst, ≥99.0%, tin content: ≥28.0 wt%, stannous content: ≥27.25 wt%) were supplied by Shandong Baixian Chemical Co., Ltd., China. Silicone oil L580 (foam stabilizer) was purchased from Momentive Performance Materials Inc., USA. C.I. Vat Yellow 1 and C.I. Vat Black 27 were purchased from Shanghai Huayuan Industrial Co., Ltd., China. Pigment paste LR22 (solid content: 44.0 wt%), L362B (solid content: 42.0–46.0 wt%) and L363A (solid content: 45.0–50.0 wt%) were purchased from Suzhou Summun Technology Co., Ltd., China. Diethanolamine (DEA, $C_4H_{11}NO_2$, ≥99.0%) and chlorophyllin sodium copper salt (CSCS, $C_{34}H_{31}CuN_4Na_3O_6$) were obtained from Shanghai Maclean Biochemical Technology Co., Ltd., China.

2.2 Preparation of polyurethane-based bionic porous substrates (BPSs)

Deionized water was used as foaming agent to prepare BPS. Polyether polyol 3050 (20 parts), silicone oil L580 (0.3 parts), DEA (0.06 parts) and different amounts (0.6 parts, 0.7 parts, 0.8 parts, 1.0 part, 1.5 parts, 2.0 parts) of foaming agent were mixed and stirred at 400 rpm for 5 min as the polyol component. The mixture of TDI 80/20 (7.6 parts) and stannous octoate T9 (0.16 parts) was used as the isocyanate component, which was further mixed with the polyol component at 500 rpm for 15–20 s. The mixture foamed in a mold (20 × 20 cm) for 5 min, then it was aged in an oven at 60 °C for 2 hours and followed by another 16–24 h at ambient temperature. Finally, the BPSs were obtained after cutting through a heating wire.

2.3 Preparation of bionic porous spectrum simulation materials (BPSSMs)

Dispersion of vat dyes and organic pigments were used as foaming agents to prepare BPSSM-VD/BPSSM-OP. The specific formula of the vat dyes dispersion was as follows: Vat Black 27 (8 parts), Vat Yellow 1 (10 parts) and different amounts (1 part, 2 parts, 3 parts, 4 parts, 5 parts) of CSCS were added to deionized water (250 parts). The specific formula of the organic pigments dispersion was as follows: LR22 (4.2 parts), L362B (15.4 parts), L363A (3.85 parts) and different amounts (1 part, 5 parts, 10 parts) of CSCS were added to deionized water (250 parts). The foaming agent was obtained after ultrasonic the dispersion for 30 min, and the BPSSM-VD/BPSSM-OP was prepared according to the preparation method in Section 2.2.

2.4 Measurements

Vis-NIR reflectance/transmittance spectra tests were performed by UV-Vis-NIR Spectrophotometer (LAMBDA 950, PerkinElmer GmbH, US). The samples were cut into 5 × 5 cm and tested at solid reflectance/transmittance measurement chamber.

Density and open porosity were measured by intelligent porous material analyzer (MAY-ML304T, Miaozhun Technology (Shenzhen) Co., Ltd., China).

Pore structures were observed by Metallographic Microscope (XY-MRT, Ningbo Sunny Instruments Co., Ltd., China) at 50 times.

Radiation temperature tests were measured by Thermal Imager (testo 871, Testo SE & Co. KGaA, Germany). BPSSM was cut into the shape of leaves and placed in the heather bush. The test time was from 5:00 am on June 10, 2019 to 5:00 am the next day. Temperature: 18–29 °C, humidity: 52–93%.

Three-dimensional configuration was recorded by three-dimensional surface topography measuring instrument (Infinite Focus SL, Alicona Imaging GmbH, Austria).

The static contact angles of water droplet on ten common leaves and BPSSM were measured with a standard contact angle meter (JC2000DM, Shanghai Zhongchen Digital Technic Aapparatus Co., Ltd, China) at ambient temperature.

The spectral correlation coefficient (r_m) was calculated by cross-correlogram spectral matching method (eqn (1)).

$$r_m = \frac{\sum_{\lambda=\lambda_a}^{\lambda_b} \left(R_{r(\lambda)} - \overline{R}_r\right)\left(R_{t(\lambda)} - \overline{R}_t\right)}{\sqrt{\sum_{\lambda=\lambda_a}^{\lambda_b} \left(R_{r(\lambda)} - \overline{R}_r\right)^2}\sqrt{\sum_{\lambda=\lambda_a}^{\lambda_b} \left(R_{t(\lambda)} - \overline{R}_t\right)^2}} \quad (1)$$

where $R_{r(\lambda)}$ and $R_{t(\lambda)}$ are the reflectance of the reference and test sample, respectively. $\bar{R}_r$ and $\bar{R}_t$ are the average reflectance of the reference and test samples in the measured spectral range (λ_a–λ_b). The range of r_m is [−1, 1], and the larger the absolute value of r_m, the more similar the spectral curve of the reference and the test sample.

Breaking strength of the composite fabric was measured with electronic fabric strength machine (YG026C, Changzhou Second Textile Machinery Co., Ltd., China) according to the ISO/DIS 13934.1-94 method at ambient temperature.

3. Result and discussion

3.1 Relationship between the structure composition and spectral properties of leaves

Fig. 1a shows the Vis-NIR spectra of ten common plant leaves, which are widely distributed in Eastern China. It can be seen that all the leaves have similar spectral curves which

incorporated into four characteristics in the region of 380–2500 nm.[19] Green apex (380–680 nm). A broad peak with moderate intensity (reflectance ranges from 8% to 16%) appearing at 550 nm in the visible region, which makes the leaves exhibit green hue. Red edge: the reflectance rises sharply from 680 nm to 780 nm and form a steep slope. Near-infrared plateau: the reflectance maintains between 40% and 60%, which can be regarded as a plateau in the spectra. Water absorption valley: two broad absorption valleys with strong intensity appearing at 1450 nm (10–30%) and 1950 nm (4–10%), respectively.

It is well known that fresh green leaves are mainly composed of epidermis, chlorophyll, mesophyll tissue and water.[20,21] In order to explore the relationship between the composition structure and the spectral characteristics, several experiments were designed to obtain the following types of leaves: green fresh leaf, yellow fresh leaf, chlorophyll-removal leaf and green dead leaf. The spectra of them were studied in Fig. 1b. Totally different spectra of two fresh leaves appear within the visible region, and green fresh leaf exhibits obvious green apex and red edge, which implies that the chlorophyll in the leaves is beneficial to forming the green apex and red edge. In order to prove this perspective, chlorophyll was removed from the leaves by immersing the leaves in anhydrous ethanol at 60 °C for 2 h. It can be seen that both of the green apex at 550 nm and red edge disappear, and the spectrum is roughly the same as yellow fresh leaf except the attenuated absorption at 1450 nm and 1950 nm due to the loss of water of leaf after heat treatment in ethanol, which confirms that the two absorptions are produced by the water in the leaves.[22–24]

Furthermore, the spectra of dried leaf and dead leaf were measured in Fig. 1c. The result shows that they both lose the four characteristics of fresh leaf due to the loss of the chlorophyll and water. And the spectra exhibit a significant difference between 700 and 1300 nm, the specific performance is the different degree of destruction of the near-infrared plateau. It is presumably attributed to that the dried leaf lose the water and become fragile due to the short heat treatment, and the porous mesophyll tissue of which is partially collapsed.[25] But the mesophyll tissue of dead leaf is totally destroyed due to senescence during seasonal changes, the difference in the spectrum is reflected in the partial destruction or complete disappearance of the near-infrared plateau. It can be speculated that the near-infrared plateau is formed by healthy and intact mesophyll tissue in the leaves.[19,26–29]

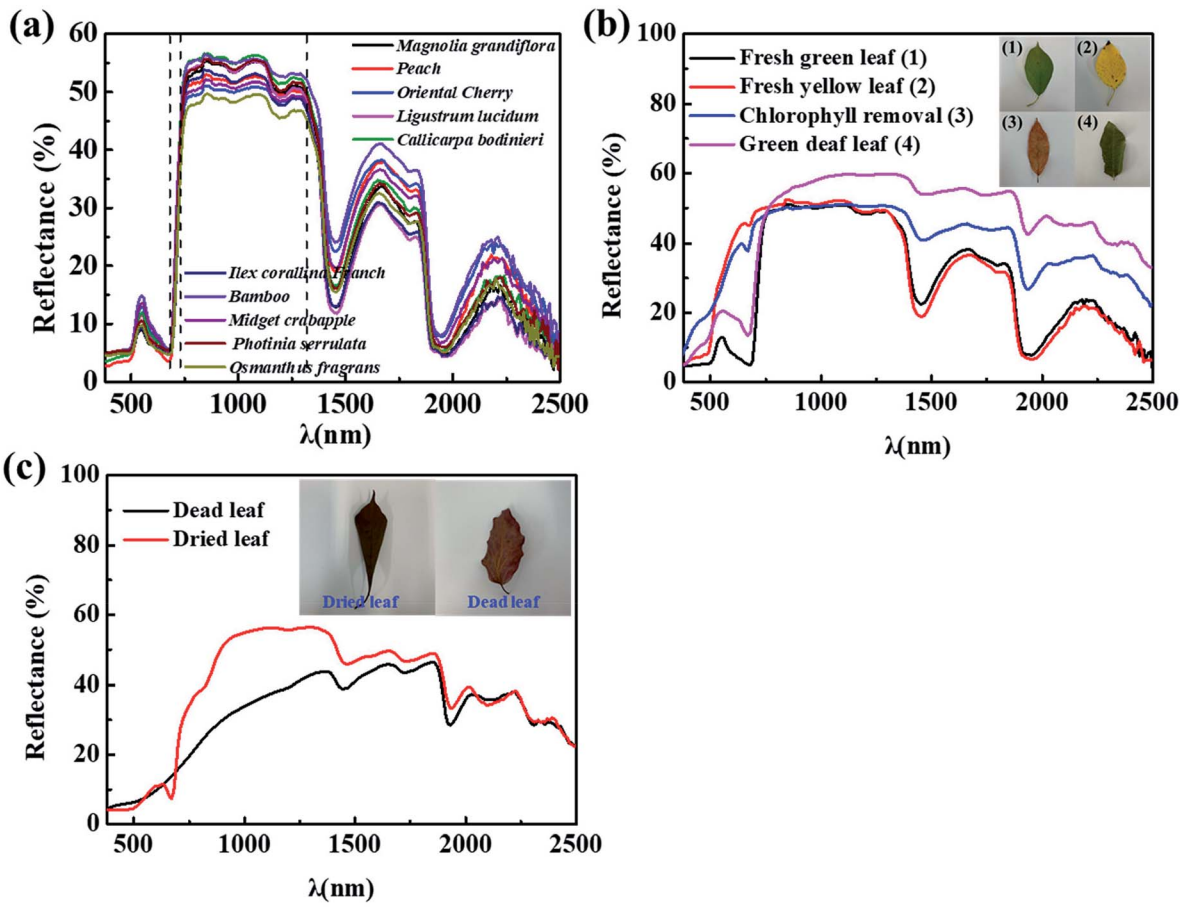

Fig. 1 The Vis-NIR spectra of (a) ten common plant leaves (*Magnolia grandiflora*, peach, oriental cherry, *Ligustrum lucidum*, *Callicarpa bodinieri*, *Ilex corallina* Franch, bamboo, *Midget crabapple*, *Photinia serrulate*, *Osmanthus fragrans*), (b) green fresh leaf, yellow fresh leaf, chlorophyll removed leaf and green dead leaf, respectively, (c) dead and dried leaf.

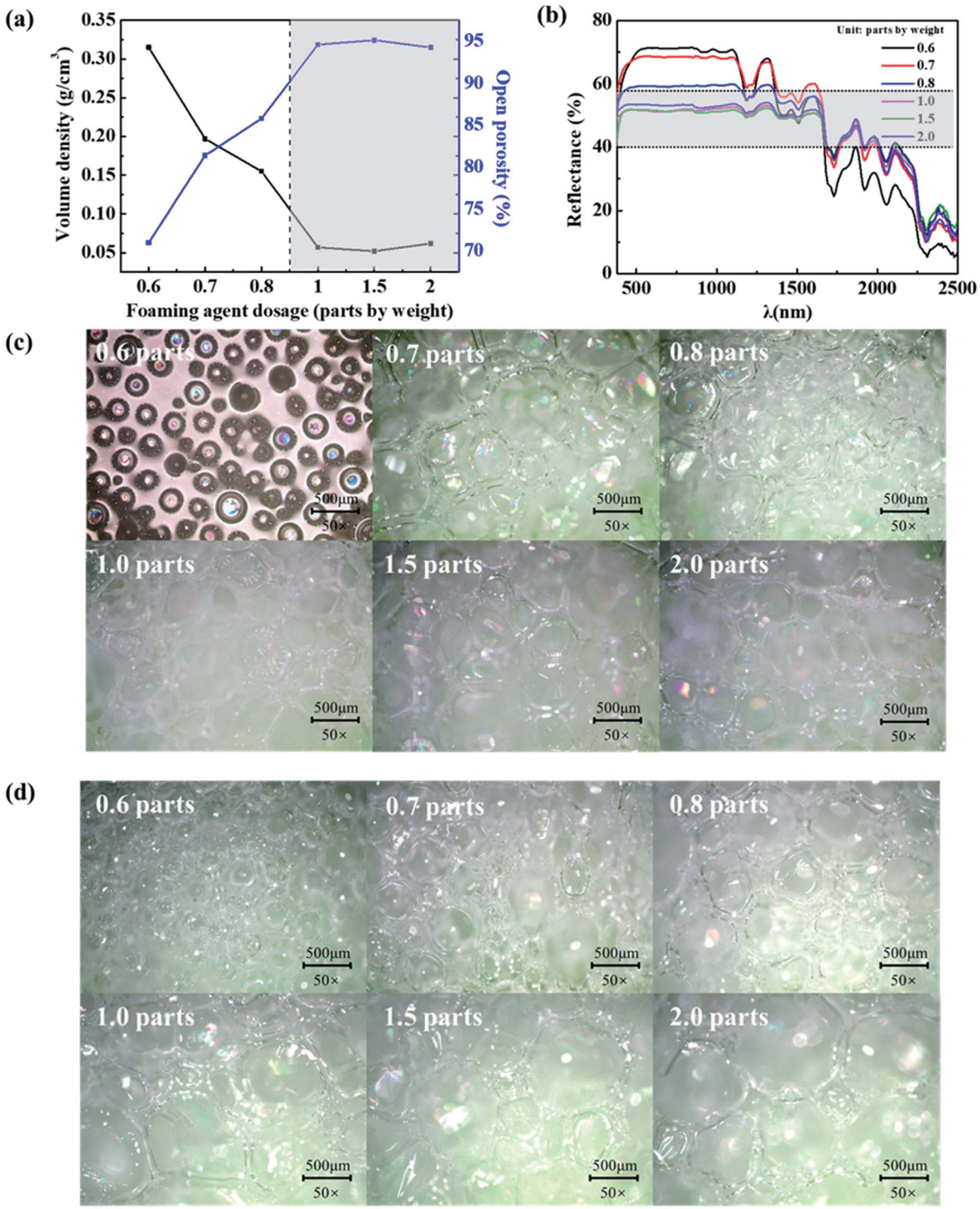

Fig. 2 The (a) volume density and open porosity, (b) Vis-NIR spectra, (c) metallographic microscope images of BPSs with different foaming agent amount, (d) metallographic microscope images of the cross section of BPSs with different foaming agent amount.

3.2 Spectral simulation of near-infrared plateau characteristic

Based on the above conclusion that the porous mesophyll tissue endows the near-infrared plateau of leaves. It is known that total transmittance, reflectance and absorptivity of the material is 100%, dense structure will cause the low transmittance and high reflectance.[30] To maintain the reflectivity between 40–60% in the range of 800–1300 nm, bionic porous substrate was used to simulate the near-infrared plateau of leaves by improving the transmittance of materials. Since foaming agent amount is one of the decisive factors to regulate the pore structures of BPSs,[31]

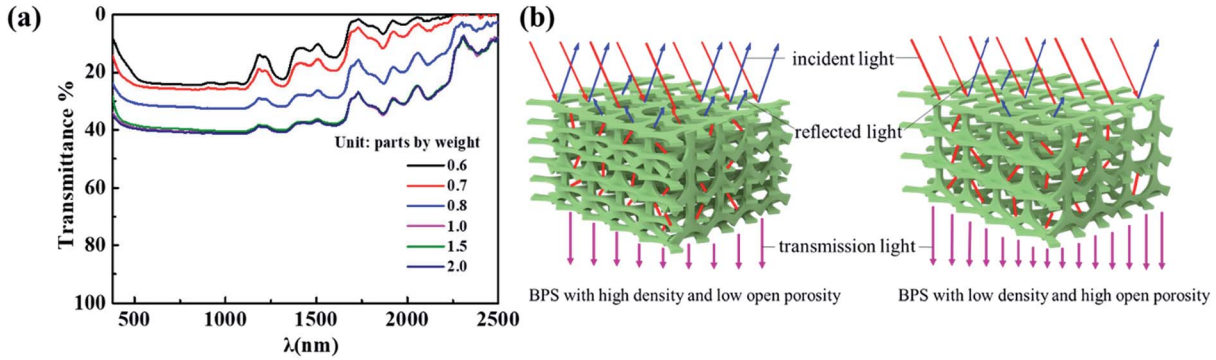

Fig. 3 The (a) transmittance spectra of BPSs with different foaming agent amount, (b) optical path model of the BPSs.

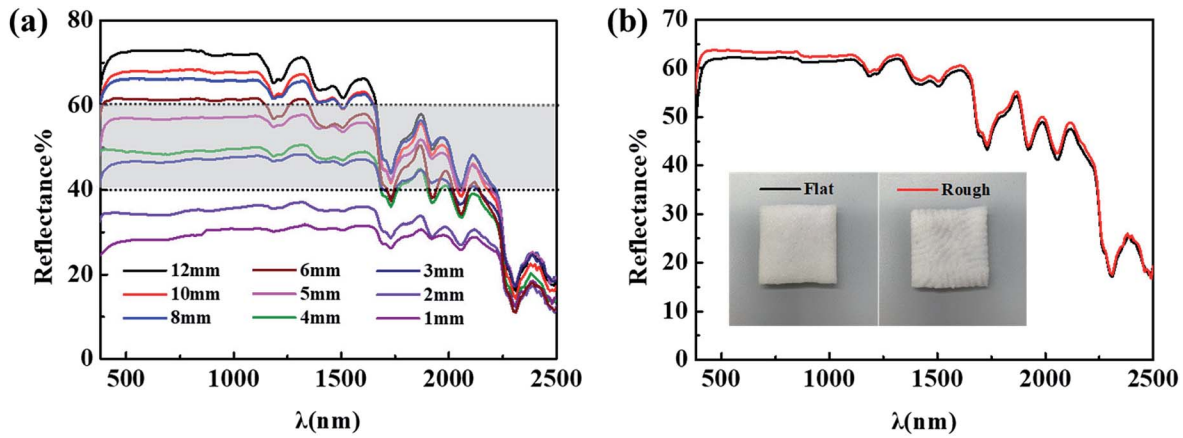

Fig. 4 The Vis-NIR spectra of BPSs with different (a) thickness and (b) surface topography.

the relationships among foaming agent, pore structure (containing size, open porosity and volume density) and near-infrared plateau in spectrum were explored. Fig. 2a shows that BPSs with low density (<0.10 g cm^{-3}) and high open porosity (>90%) can be obtained by adjusting the amount of foaming agent to more than 1.0 part. Meanwhile, the BPSs forms more

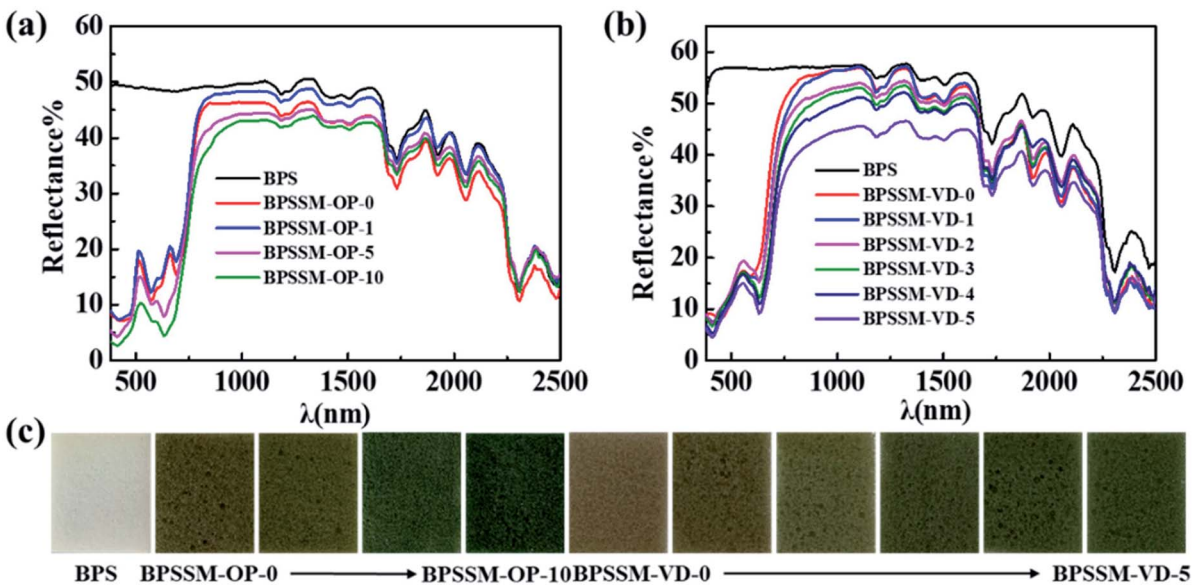

Fig. 5 The (a) Vis-NIR spectra of BPSSM-OP, (b) Vis-NIR spectra of BPSSM-VD and (c) photograph of BPSSM-OP and BPSSM-VD with different CSCS amounts. (BPSSM-XX-Y: XX represents the type of colorants; Y represents the parts of the CSCS).

open pore structures as the amount of foaming agent increases. The closed-pore structures may be due to the fact that the foaming reaction is weaker than gel reaction when use less foaming agent, thus releasing less CO_2. The amount of CO_2 gas is insufficient to break through the pore wall during the foaming process, which lead to the high density of BPS and formation of many closed-pore structures.[32] The strength of the foaming reaction is improved as the foaming agent amount increase, which lead to the formations of large amount of CO_2 and interconnected pore structures. This phenomenon eventually causes lower density and higher open porosity, respectively.[33] The above changes can be visually observed from the microscope images of the surface and cross section of the BPSs with different foaming agent amount (Fig. 2c and d).

Combined with the spectra as shown in Fig. 2b, it can be found that the pore structure of BPSs mainly affects the height of the near-infrared plateau and the absorption at 1200 nm. The reflectance of the near-infrared plateau is proportional to the density and inversely proportional to the open porosity. The pore structure of the BPSs can be regulated by the amount of foaming agent to further adjust the spectral characteristics. Lower density (<0.10 g cm^{-3}) and higher open porosity (>90%) of BPSs are beneficial to form the near-infrared plateau with about 50% reflectance, which is consistent with the spectral characteristics of natural leaves. It is speculated that the optical path of the diffusion light inside the materials is related to its thickness, size and density.[34] The transmittance will increase when the open porosity increases as shown in Fig. 3a and b, which lead to the reflectance of near-infrared plateau in spectrum decreases, as well as the weaken of the absorption at 1200 nm.

Moreover, the effects of thickness and surface topography of BPSs on the near-infrared plateau were also studied as shown in Fig. 4. The results show that the reflectance of near-infrared plateau of BPSs gradually increases with the increasing of thickness due to the reduction of transmittance.[35] The reflectance in the range of 800–1300 nm can be maintained between 40–60% by regulating the thickness of BPS within 3–5 mm, which matches with the characteristics of the near-infrared plateau of natural leaves. In addition to the thickness, BPS with a flat front and a rough back was used to study the influence of surface topography on the spectrum. The result shows that the reflectance of one side with a rough surface is slightly higher than that of the flat surface, and the impact of surface topography is negligible.

3.3 Spectral simulation of the visible region

To simulate the green apex and red edge of the natural leaves ranging in 380–780 nm, green colorants were obtained by trichromatic theory of dye mixing and used to simulate the effect of chlorophyll.[36] Several organic pigments and vat dyes were selected to obtain two system of foaming agent dispersions to prepare BPSSM-OP and BPSSM-VD. The position and slope of the green apex and red edge were further regulated by the amount of CSCS. The Vis-NIR spectra of BPSSM-OP and BPSSM-VD with different CSCS amounts are shown in Fig. 5. Compared to the BPS, the addition of organic pigments makes the BPSSM-OP-0 exhibit two reflection peaks (510 nm and 650 nm) in the visible region and show the red edge (Fig. 5a). However, the position and amount of apex are inconsistent with that of natural leaves. The increasing addition of CSCS can adjust the reflection peak at 510 nm to gradually red shift and eliminate the reflection peak at 650 nm, which is more consistent with the spectra of natural leaves in the visible region. The r_m between BPSSM-OP and natural leaves in the range of 380–1300 nm reach to 0.979 by adjusting the amount of CSCS to 5 parts. In another system of BPSSM-VD (Fig. 5b), the BPSSM-VD-0 shows a green apex at 550 nm, but the shape of which is not obvious compared with the natural leaves. The increasing addition of CSCS makes the shape of the green apex clearer, but the slope of the red edge decrease. The r_m between BPSSM-VD and the natural leaves in the range of 380–1300 nm reach to 0.980 by controlling the amount of CSCS to 3 parts.

3.4 Spectral simulation of the water absorption valley

In addition to the green apex and red edge, the simulation of water absorption valley in the spectrum of the natural leaves is also crucial.[37] The spectra of BPSSM-VD with different water content (0–150%, w/w) were collected as shown in Fig. 6. The intensity of the water absorption valley increases as the water content increases. Therefore, the intensity of the water absorption valley can be regulated by water content of the BPSSM. The water absorptions of the BPSSM-VD with 100–120% water content are consistent with the natural leaves spectral curve channel. Excessive water content lead to strong water absorption of BPSSM, which is discrepant with natural leaves.

BPSSMs with certain water contents have all the spectral characteristics of the natural leaves, which are similar with spectral characteristics of natural leaves in the 380–2500 nm band. Fig. 7 shows the reflectance spectrum of two kinds of BPSSM and natural leaves. Table 1 shows that the r_m between different leaves and BPSSMs. It can be found that the r_m between BPSSM-OP and ten leaves is more than 0.960, and 60%

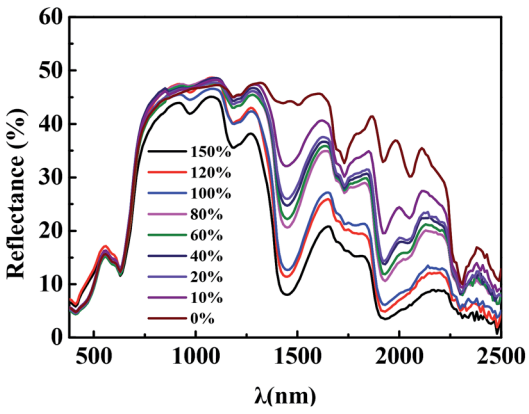

Fig. 6 The Vis-NIR spectra of BPSSM-VD with different water contents.

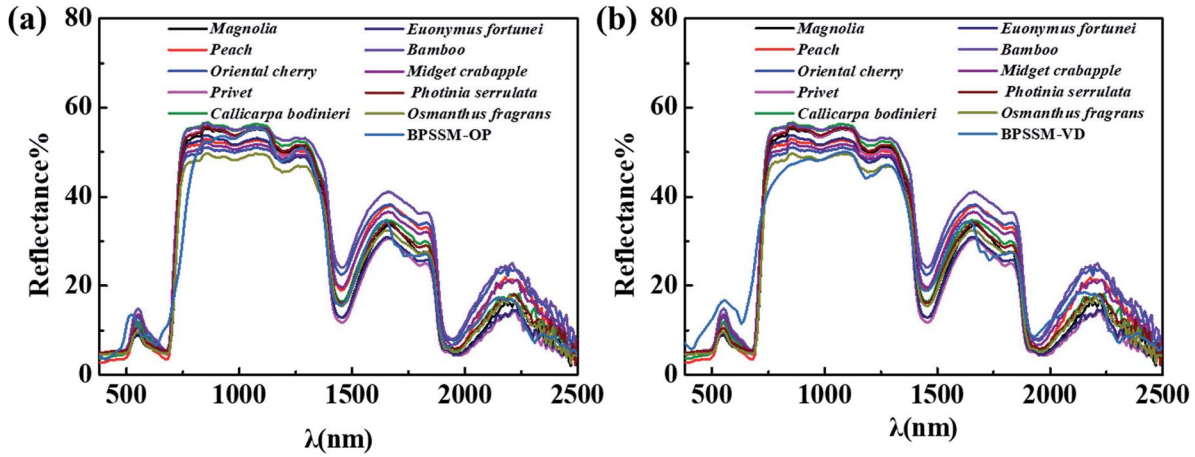

Fig. 7 Comparison of Vis-NIR spectra of (a) BPSSM-OP, (b) BPSSM-VD with ten common leaves.

Table 1 The r_m between ten common leaves and BPSSM-VD, BPSSM-OP, respectively

Names of the ten common leaves	Correlation coefficient (r_m)	
	BPSSM-OP	BPSSM-VD
Magnolia grandiflora	0.984	0.974
Peach	0.971	0.963
Oriental Cherry	0.965	0.958
Ligustrum lucidum	0.980	0.977
Callicarpa bodinieri	0.981	0.977
Ilex corallina Franch	0.983	0.976
Bamboo	0.969	0.962
Midget crabapple	0.974	0.972
Photinia serrulate	0.983	0.975
Osmanthus fragrans	0.983	0.976

of which is above 0.980. The r_m between BPSSM-VD and ten leaves is greater than 0.950, and 70% of which is above 0.970. These suggest that the BPSSM is universal in simulating the spectra of leaves.

3.5 Thermal infrared property

BPSSM was cut into the shape of leaves and placed in the heather bush. The infrared thermal images of the bush were collected by thermal infrared camera every hour from 5:00 am on June 10, 2019 to 5:00 am the next day. Fig. 8a shows that the variation trend of radiant temperature of BPSSM is consistent with natural leaves as the time extend, the average radiant temperature difference ($\Delta\bar{T}$) between them is 0.25 °C, and the maximum radiant temperature difference (ΔT_{max}) is 0.9 °C, which may be attributed to low thermal conductivity and emissivity of porous polyurethane material.[38,39] Fig. 8b shows the thermal infrared images of four typical moments in the morning (5:00), noon (11:00), evening (17:00) and late night (23:00). It can be seen that the BPSSM was well integrated with the plant background in thermal infrared images, indicating that it can simulate the thermal infrared characteristics of the natural leaves.

3.6 Morphology and hydrophobicity

The three-dimensional profiles of the surface and cross section of BPSSM were also characterized by three-dimensional profiler

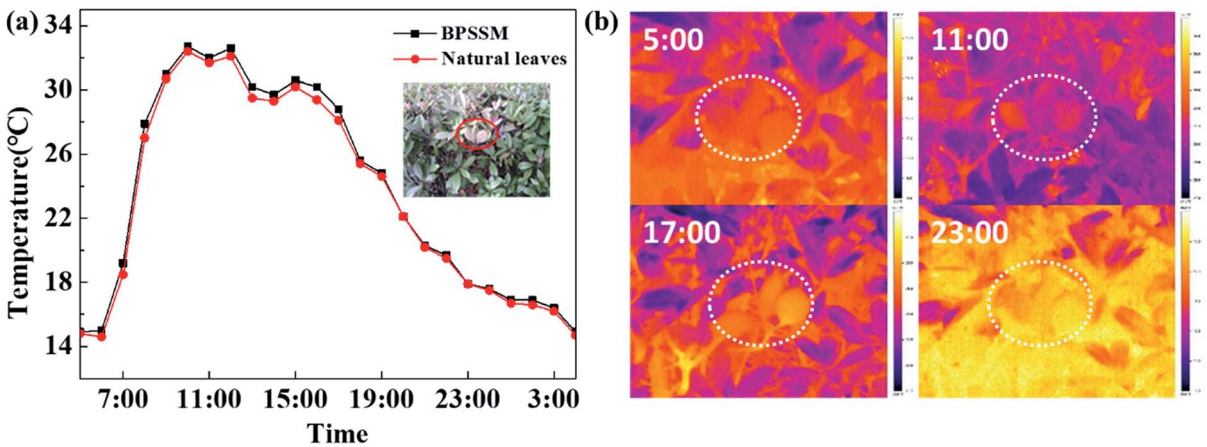

Fig. 8 The (a) radiation temperatures and (b) thermal infrared images of BPSSM in the bushes at natural environment.

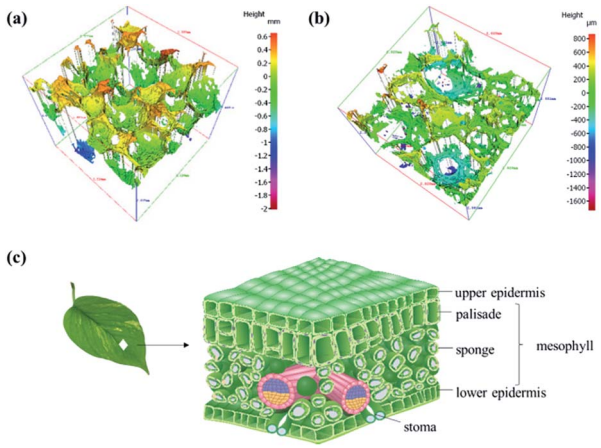

Fig. 9 (a) Three-dimensional profile of the BPSSM, (b) three-dimensional profile of the cross section of the BPSSM, (c) structure diagram of leaves.

as shown in Fig. 9a and b, the BPSSM has a complete three-dimensional porous structure with no obvious defects, and the interior structure of the BPSSM is relatively uniform. Different colours represent different heights, and the surface of the material forms a high and low undulating surface due to its skeleton.[40] Fig. 9b shows the internal structure diagram of natural leaves. The gaps between the mesophyll cells constitutes a ventilation system, the cells are arranged loosely and the gap is wide especially in the sponge tissue.[41] From structural perspective, there is a certain similarity between BPSSM and mesophyll tissue of leaves, which may be the reason why it can simulate the spectral characteristics of mesophyll tissue.

The static contact angles of water droplet on the surfaces of the ten common leaves and BPSSM were shown in Fig. 10. The contact angles of water droplet on ten common leaves are between 55–95°, and the contact angle of BPSSM is 106.5°, which is slightly higher than natural leaves and indicated its hydrophobic surface. It may be attributed that the chemical composition of polyurethane-based porous material is non-polar and repels polar water droplets. Moreover, the three-

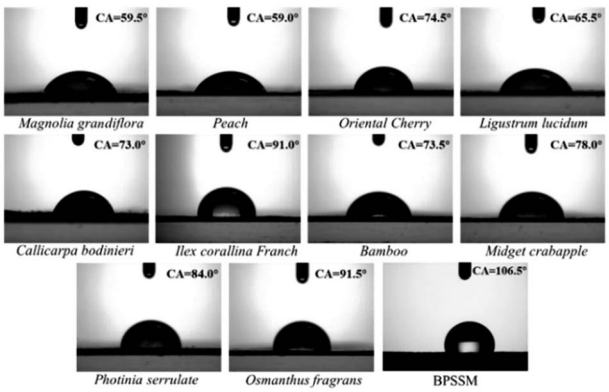

Fig. 10 The contact angels of the ten common leaves and BPSSM.

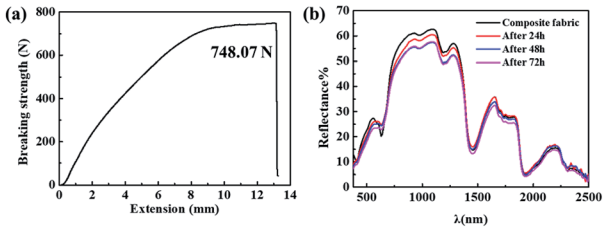

Fig. 11 (a) Stress–strain curve, (b) photostability of composite fabric.

dimensional structure of BPSSM can also reduce the effective contact area between its surface and the water droplets, and the contact with the water droplets can be regarded as a kind of composite contact, thus the BPSSM exhibits good hydrophobicity.[42] The special hydrophobic surface of BPSSM can prevent it from absorbing excessive water on rainy days to some extent, resulting in overweight and strong water absorption in spectrum of material.

To improve the application performance of BPSSM, it was combined with acrylic fabric to prepare composite fabric. The stress–strain curve and the spectrum of composite fabric were shown in Fig. 11. The results show that the breaking strength of composite fabric is 748.07 N (Fig. 11a), which meet the standards of fabric applications. The spectrum of composite fabric exhibits similar spectrum with natural leaves. Moreover, the durability of composite fabric in natural environment has been conducted as shown in Fig. 11b, it can be seen that the reflectance of the BPSSM decreases as the time extended, the spectra of composite fabric after exposure natural environment for 72 h still have similar spectral characteristics to natural leaves.

4. Conclusions

Based on the investigation of the relationship between structure composition and spectra of natural leaves, a bionic porous spectrum simulation material (BPSSM) with similar spectral properties to leaves within 380–2500 nm was designed and prepared. The polyurethane-based bionic porous substrate (BPS) was used to simulate mesophyll tissue of leaves, BPS with low density (<0.10 g cm^{-3}) and high open porosity (>90%) can form the similar near-infrared plateau to leaves. Vat dyes and organic pigments were used to simulate the chlorophyll in leaves, and the spectra similarity in visible region were improved by chlorophyllin sodium copper salt. BPSSM with 100–120% water contents could simulate four key spectral characteristics of natural leaves. The high spectral correlation coefficient (r_m up to 0.984) between BPSSM and various natural leaves suggests the universality of BPSSM in simulating the spectra of leaves. In addition, the BPSSM can be well integrated with the plant background in the thermal infrared image with average radiant temperature difference of 0.25 °C, exhibiting similar thermal infrared property to natural leaves. The BPSSM is expected to be combined with textiles to obtain composite fabric against hyperspectral detection.

Conflicts of interest

There are no conflicts to declare.

Acknowledgements

This research was supported by the Natural Science Foundation of Jiangsu Province [BK20191334], Scientific Research Projects of Jiangsu Province [BY2016022-31], China Postdoctoral Science Foundation Funded Project [2018M630520], National Natural Science Foundation of China [No. 21808086], Fundamental Research Funds for the Central Universities [JUSRP21933]. Thanks also to Jiangnan University for supporting the course of research.

Notes and references

1 Y. Xu, H. Ma and S. Peng, *Ore Geol. Rev.*, 2014, **56**, 584–595.
2 M. Wahabzada, A. K. Mahlein, C. Bauckhage, U. Steiner, E. C. Oerke and K. Kersting, *Sci. Rep.*, 2016, **6**, 22482.
3 P. Thenkabail, *Hyperspectral remote sensing of vegetation*, 2008.
4 D. Manolakis, D. Marden and G. A. Shaw, *Linc. Lab. J.*, 2003, **14**(1), 79–116.
5 H. Zhang and J. Zhang, *J. Text. Res.*, 2007, **28**, 60–63.
6 M. K. Mehrizi, S. Mallakpour, S. M. Bidoki, M. Vik and M. Vikova, *Fibers Polym.*, 2012, **13**, 501–506.
7 K. K. Gupta, A. Nishkam and N. Kasturiya, *J. Ind. Text.*, 2001, **31**, 27–42.
8 U. Goudarzi, J. Mokhtari and M. Nouri, *Color Res. Appl.*, 2014, **39**, 200–207.
9 Z. Liu, W. Wu and B. Hu, *Sci. China, Ser. E: Technol. Sci.*, 2008, **51**, 1902–1910.
10 Y. Yang, Z. Liu, B. Hu, Y. Man and W. Wu, *J Bionic Eng*, 2010, **7**, S43–S49.
11 R. Qin, G. Xu, L. Guo, Y. Jiang and R. Ding, *Mater. Chem. Phys.*, 2012, **136**, 737–743.
12 F. Zhao, R. Li, W. Verhoef, S. Cogliati, X. Liu, Y. Huang, Y. Guo and J. Huang, *Remote Sens. Environ.*, 2018, **219**, 233–246.
13 R. Sato, H. Ito and A. Tanaka, *Photosynth. Res.*, 2015, **126**, 249–259.
14 S. Liang, H. Zhang, M. Luo, K. Luo, P. Li, H. Xu and Y. Zhang, *Ceram. Int.*, 2014, **40**, 4367–4373.
15 R. Levinson, P. Berdahl and H. Akbari, *Sol. Energy Mater. Sol. Cells*, 2005, **89**, 351–389.
16 G. Ying and Y. Hong, *Int. J. Heat Mass Transf.*, 2017, **114**, 115–124.
17 P. Li, H. Xu, S. Zheng, Y. Zhang, Z. Li and Y. Bai, *Environ. Sci. Technol.*, 2008, **42**, 7231.
18 L. M. Pedersen and H. Permin, *Lancet*, 1988, **331**, 1267–1269.
19 E. B. Knipling, *Remote Sens. Environ.*, 1970, **1**, 155–159.
20 *Plant biochemistry*, ed. J. Bonner and J. E. Varner, Elsevier, 2012.
21 W. G. Hopkins, *Introduction to plant physiology*, John Wiley and Sons, 2nd edn, 1999.
22 H. Chang, H. Wu, T. Chen, K. Huang, C. Jwo and Y. Lo, *J. Alloys Compd.*, 2010, **495**(2), 606–610.
23 D. A. Sims and J. A. Gamon, *Remote Sens. Environ.*, 2003, **84**, 526–537.
24 D. A. Sims and J. A. Gamon, *Remote Sens. Environ.*, 2002, **81**, 337–354.
25 N. Therdthai and W. Zhou, *J. Food Eng.*, 2009, **91**(3), 482–489.
26 S. Gürtler, C. Souza Filho, I. Sanches, M. Alves and W. Oliveira, *ISPRS J. Photogrammetry Remote Sens.*, 2018, **146**, 272–288.
27 P. Lim, H. Kim and H. Nam, *Annu. Rev. Plant Biol.*, 2007, **58**, 115–136.
28 A. M. Fischer, *Annual Reviews of Senescence Processes in Plants*, 2007, vol. 26, pp. 87–107.
29 A. Maria, G. Lo, N. Andrea, T. Patrizia and S. Sebastiano, *Tree Physiol.*, 2005, **25**(4), 505–512.
30 E. Hecht, *Optics*, Pearson, 2015.
31 C. Zhang, J. Li, H. Zhen, F. Zhu and Y. Huang, *Mater. Des.*, 2012, **41**, 319–325.
32 J. Zhang, N. Hori and A. Takemura, *Polymer Degradation and Stability*, 2019, p. 166.
33 P. Cinelli, I. Anguillesi and A. Lazzeri, *Eur. Polym. J.*, 2013, **49**, 1174–1184.
34 J. S. Shenk, J. J. Workman and M. O. Westerhaus, *Handbook of Near-Infrared Analysis*, 2008.
35 D. Baillis, M. Arduini-Schuster and S. Jean-Francois, *ICHMT Digital Library Online*, Begell House Inc., 2001.
36 J. Cohen, *Visual color and color mixture: The fundamental color space*, University of Illinois Press, 2001.
37 Q. Zhang, Q. Li and G. Zhang, *J. Spectrosc.*, 2012, **27**(2), 93–105.
38 A. Bouchair, *Build. Environ.*, 2008, **43**(10), 1603–1618.
39 R. C. Progelhof, J. L. Throne and R. R. Ruetsch, *Polym. Eng. Sci.*, 1976, **16**(9), 615–625.
40 S. Ma, R. Zhu, C. Quan, L. Chen, C. Tay and B. Li, *Appl. Opt.*, 2012, **51**(13), 2419–2428.
41 L. Sack and C. Scoffoni, *New Phytol.*, 2013, **198**(4), 983–1000.
42 Q. Zhu, Y. Chu, Z. Wang, N. Chen, L. Lin, F. Liu and Q. Pan, *J. Mater. Chem. A*, 2013, **1**(17), 5386–5393.

